Transactions on Metals and Alloys (2022)
Clausius Scientific Press, Canada

DOI: 10.23977/trama.2022.010101
ISSN 2616-2466 Vol. 1 Num. 1

Structure and Magnetic Studies of Gadolinium Doped M-type Barium Hexagonal Ferrite

Kaimin Su[1], Kai Yuan[1], Zeping Guo[1,*], Yun He[2,*]

[1]College of Physics and Technology, Guangxi Normal University, Guilin 541004, China.
[2]Guangxi Key Laboratory of Nuclear Physics and Nuclear Technology, Guangxi Normal University, Guilin 541004, China.
**corresponding author*

Keywords: $Ba_{1-x}Gd_xFe_{12}O_{19}$, Doping, Magneto-plumbite type ferrite, Magnetic properties, Particle size.

Abstract: The sol-gel self-propagation method was used to dope different kinds of Gd ions on M-type $Ba_{1-x}Gd_xFe_{12}O_{19}$ ferrite. The results of XRD showed that the samples are magneto-plumbite type ferrite, lattice parameter decreases gradually with Gd^{3+} ions concentration increasing, the crystal axis ratio c/a ranges from 3.9374 to 3.9772.The FT-IR analysis showed that in the vicinity of 587cm^{-1}, 545cm^{-1} and 437cm^{-1}, three obvious characteristics of M ferrite appear, indicating the samples are single phase magnetoplumbite structure. The VSM analysis showed that the specific saturation magnetization the remanence magnetization of samples decreased with Gd^{3+} ions concentration increasing, but the coercivity increased with Gd^{3+} ions concentration increasing. The SEM analysis showed that particle sizes were uniform and good dispersion, the particle size was 180nm with Gd^{3+} ions concentration increasing, and all the samples belong to the nanoparticles.

1. Introduction

Since the advent of permanent ferrites, people have been striving for high-performance products. Through more than 50 years of research and development, the various magnetic parameters of the hard ferrite can be improved to a considerable extent by various process parameters of the improved production of hard ferrite, but the difference from the theoretical value is still relatively large[1-4]. Therefore, people have chosen a new method, which is the ion substitution technology to improve the magnetic properties of hard ferrite. Therefore, the use of ion substitution technology to improve the magnetic properties of permanent ferrite has become an effective way to improve the performance of permanent ferrite materials. Many reports have recently shown that rare earth (Re) substituted M hexaferrites have improved magnetic properties[5-6]. The improvement is largely associated with the increase of both magnetocrystalline anisotropy and coercive field and magnetization observed in La-doped strontium hexaferrites. Wang et al.[7] and Lechevallier et al.[8] reported the substitution of Sm ions giving fine M ferrite powders resulting in increases in coercive field. In this paper, the sol-gel self-propagation method was used to dope different kinds of Gd ions on M-type $BaFe_{12}O_{19}$ ferrite, and the effect of Gd ion substitution on the microstructure and magnetic properties of barium ferrite was studied.

2. Experiment Section and Synthesis

$Ba_{1-x}Gd_xFe_{12}O_{19}$ (x=0.00 , 0.05 , 0.10 , 0.15 , 0.20 , 0.25) nanoparticles were prepared by a sol-gel auto-combustion method.The XRD, FT-IR, SEM and VSM were used to investigate the microstructure and magnetic properties of $Ba_{1-x}Gd_xFe_{12}O_{19}$.

3. Results and Discussion

3.1. XRD Patterns and Structures Analysis

Figure 1 is a diffraction pattern of the phase composition of the sample by X-ray diffractometry (XRD). It can be seen that the diffraction peaks of the obtained crystals are very sharp, indicating that the crystal growth in the sample is relatively complete. After comparison with the M-type ferrite standard X-ray diffraction card (PDF #27-1029), it was found that the main crystal phase in the sample was consistent with the crystal phase of the hexagonal $BaFe_{12}O_{19}$ (BaM) ferrite[9-11]. When the doping amount exceeds a certain value (x>0.15), the a-Fe_2O_3 heterophase appears at about 33 to 34 degrees. According to the Schemer formula, the average grain size of the prepared barium ferrite is around 50 nm.

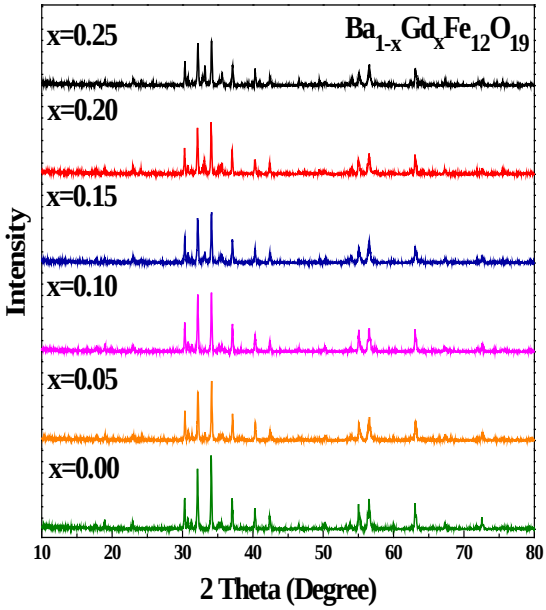

Figure 1: XRD of Ba1-xGdxFe12O19.

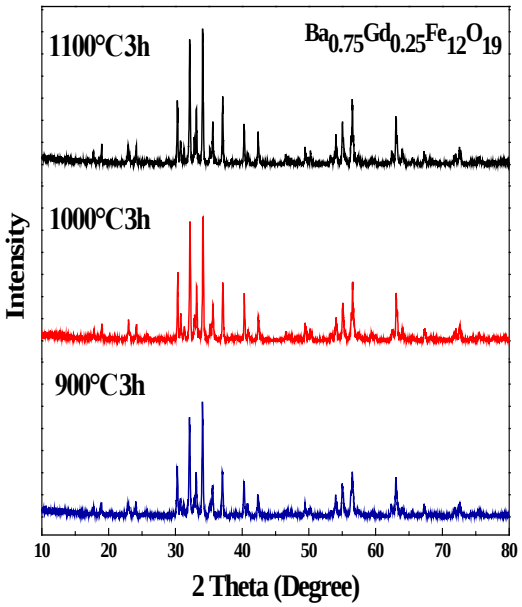

Figure 2: XRD of Ba0.75Gd0.25Fe12O19.

Figures 2, 3 and 4 shows XRD of $Ba_{0.75}Gd_{0.25}Fe_{12}O_{19}$, $Ba_{0.85}Gd_{0.15}Fe_{12}O_{19}$, $Ba_{0.95}Gd_{0.05}Fe_{12}O_{19}$ samples respectively treated at 900～1100℃ for 3h. Compared with the standard patterns given in International Centre for Diffraction Data (ICDD) files, the XRD patterns all exhibit Hexagona structure of $BaFe_{12}O_{19}$ (BaM) (file no: JCPDS#27-1029). At the same time, one can observe that the crystallization of samples is more complete as the annealing temperature is increased,and the others are no marked changes. We can conclude that Hexagona structure of $Ba_{1-x}Gd_xFe_{12}O_{19}$ can be formed at 1000 ℃ and 1100 ℃.Table 1 shows that the crystal lattice constant a of the $Ba_{1-x}Gd_xFe_{12}O_{19}$ M type ferrite magnetic powder does not change significantly with the increase of the Gd^{3+} substitution amount, and the lattice constant c generally decreases. The reason for the decrease may be related to Gd^{3+} (0.0938nm). The ionic radius is related to the small ionic radius of

Ba^{2+} (0.135nm). In addition, the crystal axial ratio c/a decreases with the increase of Gd^{3+} substitution.

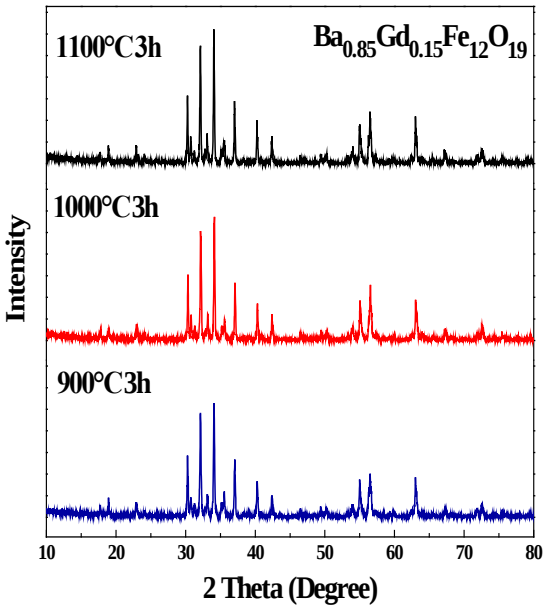

Figure 3: XRD of Ba0.85Gd0.15Fe12O19.

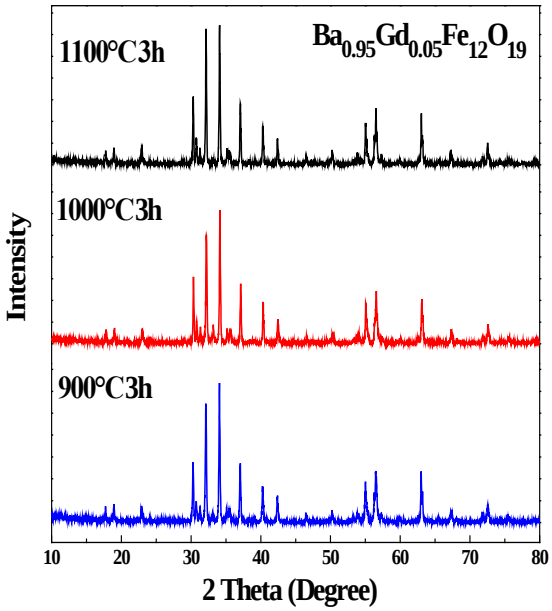

Figure 4: XRD of Ba0.95Gd0.05Fe12O19.

Table 1: XRD parameters of Ba1-xGdxFe12O19 calcined at 1000°C for 3h.

Sample(*x*)	a (Å)	b(Å)	c(Å)	c/a
0.00	5.89401	5.89401	23.23718	3.9425
0.05	5.88855	5.88855	23.22009	3.9410
0.10	5.89183	5.89183	23.21580	3.9411
0.15	5.89255	5.89255	23.20749	3.9384
0.20	5.89446	5.89446	23.24437	3.9772
0.25	5.88933	5.88933	23.18898	3.9374

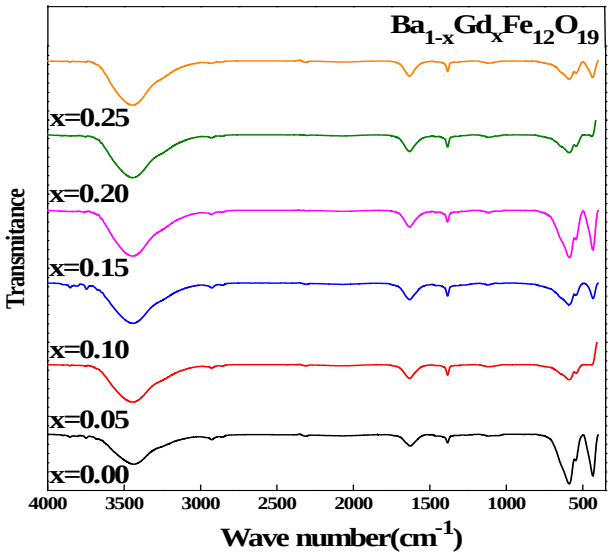

Figure 5: FT-IR of Ba1-xGdxFe12O19.

Fig. 5 shows the FT-IR spectra of $Ba_{1-x}Gd_xFe_{12}O_{19}$ (x=0.00, 0.05, 0.10, 0.15, 0.20, 0.25) samples. In the spectra as there are two bands at 3400cm^{-1} and 1644cm^{-1}, respectively, which can be assigned to the vibrations of the liquid H_2O and the variable angle. And there are three bands at 587 cm^{-1}, 545 cm^{-1} and 437 cm^{-1} which can be assigned to the vibrations of the group between Oxygen ion and metal ion in the $Ba_{1-x}Gd_xFe_{12}O_{19}$. They are character bands of the Hexagona structure of BaM ferrite. This result is consistent with the result of XRD. Compared with $BaFe_{12}O_{19}$, samples of Gd doped shows no obvious redshift and blueshift.

3.2. Magnetic property of particles

Figure 6 shows the hysteresis loops of the sample $Ba_{1-x}Gd_xFe_{12}O_{19}$ at room temperature. From the hysteresis loop diagram, we can see that the area around the hysteresis loop decreases with the increase of x, so the hysteresis loss is gradually decreasing. From Table 2, the area of hysteresis loop decreases with the increasing of the content of Gd^{3+}, which shows that the hysteresis loss is gradually reduced. It can be seen that the residual magnetization shows a more obvious decreasing trend, while the coercivity shows a more obvious increasing trend. For hexagonal ferrites, because it is a single domain structure, the demagnetization process is the rotation process of domain magnetic moment, and the main factor affecting domain rotation is the magnetocrystalline anisotropic energy. The magnetocrystalline anisotropic field, coercivity depends on the magnetocrystalline anisotropy of a single ion. The magnetocrystalline anisotropy is related to the spin-orbit coupling (relativistic effect), and the coupling strength is related to the electron motion.

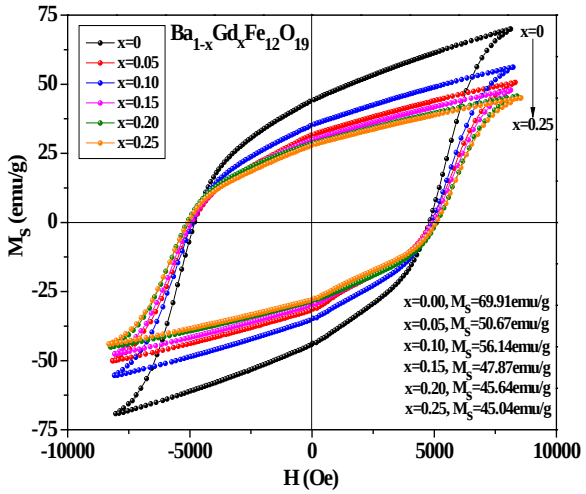

Figure 6: Hysteresis of Ba1-xGdxFe12O19.

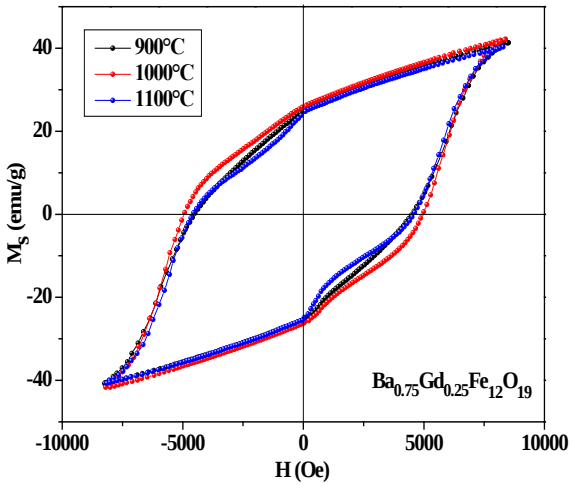

Figure 7: Hysteresis of Ba0.75Gd0.25Fe12O19.

Table 2: Magnetic parameters of Ba1-xGdxFe12O19 calcined at 1000℃ for 3h.

Sample(*x*)	M_s (emu/g)	M_r (emu/g)	H_c (Oe)
0.00	69.91	44.09	4799
0.05	50.67	31.67	4876
0.10	56.14	35.19	4886
0.15	47.87	29.85	4945
0.20	45.64	28.49	5109
0.25	45.04	27.89	5085

The orbital radius and the orbital quantum number are directly related.From Table 3, the saturation magnetization(Ms) ,the remanence(Mr) and the coercivity(Hc) of the samples all first increase then decrease with the increase of sintering temperature.

Table 3: Magnetic parameters of Ba0.75Gd0.25Fe12O19 calcined at 900℃~1100℃ for 3h.

Temperature(℃)	M_s (emu/g)	M_r (emu/g)	H_c (Oe)
900	41.32	24.99	4510
1000	42.14	25.87	4646
1100	40.28	24.26	4580

Table 4: Magnetic parameters of Ba0.85Gd0.15Fe12O19 calcined at 900℃~1100℃ for 3h.

Temperature(℃)	M_s (emu/g)	M_r (emu/g)	H_c (Oe)
900	50.90	31.13	4574
1000	50.67	31.67	4876
1100	52.22	32.38	4923

Table 5: Magnetic parameters of Ba0.95Gd0.05Fe12O19 calcined at 900℃~1100℃ for 3h.

Temperature(℃)	M_s (emu/g)	M_r (emu/g)	H_c (Oe)
900	44.93	27.22	4663
1000	47.87	29.85	4945
1100	45.79	28.17	4933

From Table 4, the saturation magnetization (Ms) ,the remanence (Mr) and the coercivity (Hc) of the samples all first increase then decrease with the increase of sintering temperature. Fig.7 and Fig.8 show the hysteresis loops of $Ba_{0.75}Gd_{0.25}Fe_{12}O_{19}$ and $Ba_{0.85}Gd_{0.15}Fe_{12}O_{19}$ at room temperature at different calcination temperatures. From the hysteresis loop diagram, it can be seen that the area around the hysteresis loop does not change very much with the increase of calcination temperature, but it can also be seen that the area of the loop is the largest at 1000℃, so the hysteresis loss is the largest at 1000℃.

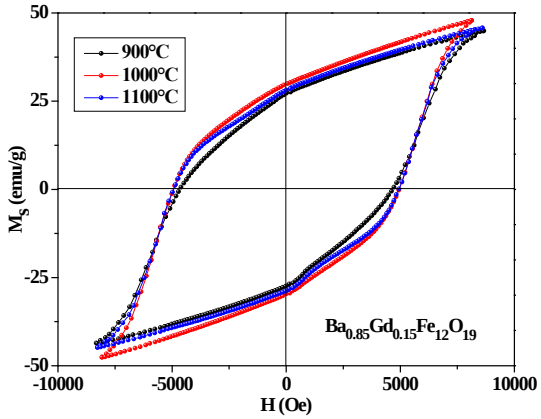

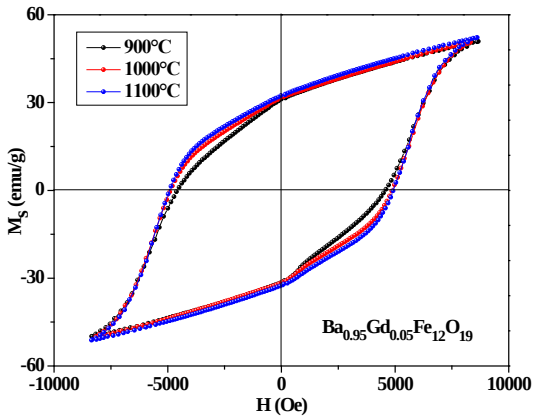

Figure 8: Hysteresis of Ba0.85Gd0.15Fe12O19. Figure 9: Hysteresis of Ba0.95Gd0.05Fe12O19.

Figure 9 shows the hysteresis loops of $Ba_{0.95}Gd_{0.05}Fe_{12}O_{19}$ at room temperature at different calcination temperatures. From the hysteresis loop diagram, it can be seen that the area around the hysteresis loop increases with the increase of calcination temperature. It can be seen that the area of the loop is the largest at 1100℃, so the hysteresis loss is the largest at 1100℃.From Table 5, the saturation magnetization (Ms) ,the remanence (Mr) and the coercivity (Hc) of the samples all gradually increase with the increase of sintering temperature.

3.3. Structures and Grain Size

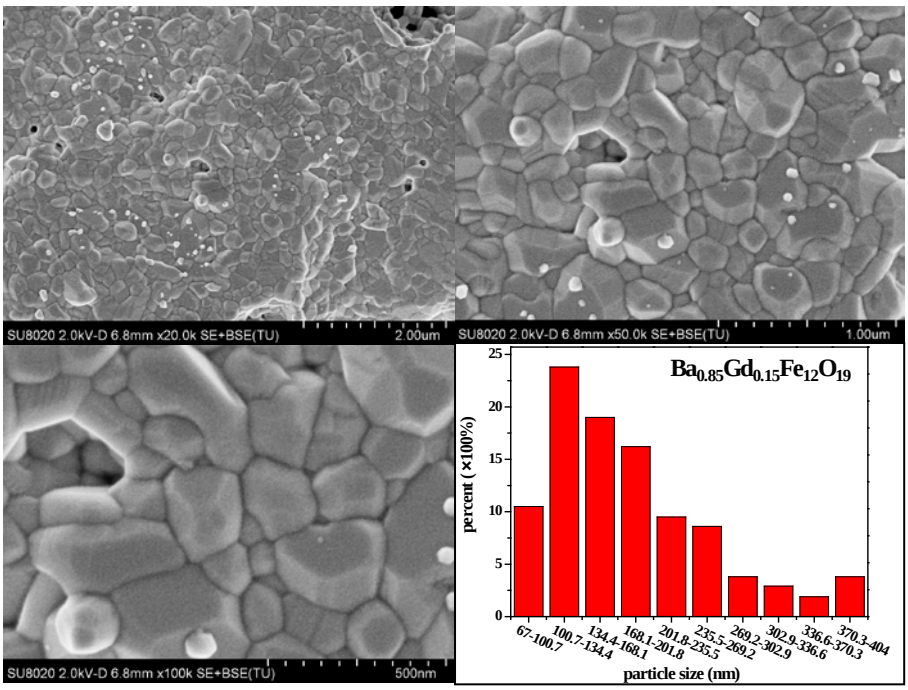

Figure 10: Size distribution of Ba0.85Gd0.15Fe12O19.

Fig.10 is the electron microscopic picture and size distribution histogram of $Ba_{0.85}Gd_{0.15}Fe_{12}O_{19}$. The grain size of sintered samples is relatively uniform, but there are a small number of unknown particles relative to $BaFe_{12}O_{19}$ samples, the average grain size is 180 nm, and the grain development is relatively adequate. From the size distribution histogram and statistical results, it can be seen that with the increase of Gd^{3+} ions, the grain size increases from 166 nm to 180 nm, and the grain size tends to increase. Scanning electron microscopy photographs show that the morphology of the samples has not changed significantly, indicating that the doping of Gd^{3+} ions has entered the lattice without changing the microstructure of barium ferrite.

4. Conclusion

In this paper, we compose a series of Gd^{3+} doped Barium Ferrite $Ba_{1-x}Gd_xFe_{12}O_{19}$ (x=0.00 , 0.05 , 0.10 , 0.15 , 0.20 , 0.25) nano-particles via sol-gel auto-combustion method. The XRD analysis showed that the samples calcined at 1000℃ for 3h are magnetoplumbite structure when x which symbolize the content of Gd is less than 0.10. But when x is larger than 0.10, the Impurity phase, a-Fe_2O_3, appear in 33 ~ 34 degrees. The lattice parameter decreased with Gd^{3+} ions concentration increasing. The results of infrared spectrum analysis are consistent with the results of XRD spectra, that the samples are single phase magnetoplumbite structure. The VSM analysis showed that the saturation magnetization of samples decreased with Gd^{3+} ions concentration increasing, but the coercivity increased with Gd^{3+} ions concentration increasing. And the saturation magnetization (M_s), the remanence (M_r) and the coercivity (Hc) of the samples all gradually increase with the increase of sintering temperature. The SEM analysis showed that particle sizes were uniform and good dispersion, the particle size increased with Gd^{3+} ions concentration increasing, and all the samples belong to the nanoparticles.

Acknowledgements

This work was financially supported by the National Natural Science Foundation of China (NO.12164006, 11364004) and Guangxi Key Laboratory of Nuclear Physics and Nuclear Technology. Kaimin Su and Kai Yuan contributed equally to this work.No potential conflict of interest was reported by the authors.

References

[1] W.Y. Fu, H.B. Yang, Q.J. Yu, et al. Preparation and magnetic properties materials of SrFe12O19/SiO2 nanocomposites with core-shell structure. Materials letters 61(2007):2187-2190.

[2] S. Alamolhoda, S.A. Seyyed, Ebrahimi, A. Badiei, A study on the formation of strontium hexaferrite nanopowder by a sol-gel auto-combustion method in the presence of surfactant. Journal of Magnetism and Magnetic Materials. 303(2006):69-72.

[3] P. Shi, H. How, X. Zuo, et al. Application of Single-Crystal Scandium Substituted Barium Hexagonal for Monolithic Millimeter-Wavelength Circulator. IEEE Transaction on Magnetics, 2001, 37(6):3941-3496.

[4] S. Ounnunkad, Improving Magnetic Properties of Barium Hexaferrites by La or Pr Substitution. Solid state Communications, 2006, 138(9): 472-475.

[5] G. Murtaza Rai, M.A. Iqbal, K.T. Kubra, Effect of Ho3+ Substitutions on the Structural and Magnetic Properties of BaFe12O19 Hexaferrites. Journal of Alloys and Compounds, 2010, 495(1):229-233.

[6] M. Kupferling, V. Corral Flores, R. Grossinger, J. Matutes Aquino. Preparation and characterization of LaFe12O19 hexaferrite. Journal of Magnetism and Magnetic Materialser, 2005, 290-291:1255-1258.

[7] J.F. Wang, C.B. Ponton, I.R. Harris. A study of Sm-substituted SrM magnets sintered using hydrothermally synthesized powders. Journal of Magnetism and Magnetic Materials, 2006,298 (2):122-131.

[8] L. Lechevallier, J.M. Le Breton, J.F. Wang, I.R. Harris. Structural analysis of hydrothermally synthesized Sr1-xSmxFe12O19 hexagonal ferrites. Journal of Magnetism and Magnetic Materials, 2004, 269(2):192-196.

[9] C.J. Li, B. Wang, J.N. Wang. Magnetic and microwave absorbing properties of electrospun Ba(1-x)LaxFe12019 nanofibers. Journal of Magnetism and Magnetic Materialser, 2012, 324:1305-1311.

[10] X.S. Liu, W. Zhong, S. Yang, Z. Yu, B.X. Gu, Y.W. Du, Influence of La3+ substitution on the structure and magnetic properties of M-type strontium ferrites . Journal of Magnetism and Magnetic Materialser, 2002, 238:207-214.

[11] N.V. Seshamma, S. Chandra, D. Ravinder, Thermoelectric power studies of La3+ substituted strontium hexagonal ferrites . Journal of Alloys and Compound, 2006, 421:1-3.